Journal of Alloys and Compounds 628 (2015) 352–356

Contents lists available at ScienceDirect

Journal of Alloys and Compounds

journal homepage: www.elsevier.com/locate/jalcom

Synthesis and luminescent properties of two different Y_2WO_6:Eu^{3+} phosphor phases

Jaime Llanos [a,*], Douglas Olivares [a], Víctor Manríquez [b], Darío Espinoza [b], Ivan Brito [c]

[a] Departamento de Química, Universidad Católica del Norte, Avda. Angamos 0610, Antofagasta, Chile
[b] Departamento de Química, Universidad de Chile, Las Palmeras 3425, Santiago, Chile
[c] Departamento de Química, Universidad de Antofagasta, Campus Coloso, Antofagasta, Chile

ARTICLE INFO

Article history:
Received 24 September 2014
Received in revised form 5 December 2014
Accepted 16 December 2014
Available online 31 December 2014

Keywords:
Inorganic materials
Optical materials
Photoluminescence
Aurivillius phases

ABSTRACT

In this paper, two different $Y_{2-x}Eu_xWO_6$ phases were synthesized. The monoclinic phase was prepared via a conventional solid-state reaction, whereas the orthorhombic phase was obtained via a facile, low-temperature combustion synthesis method. X-ray diffraction (XRD), scanning electron microscopy (SEM), differential scanning calorimetry (DSC), and photoluminescence (PL) spectroscopy were used to characterize the resulting phosphors. The XRD results indicate the orthorhombic phase crystallized isostructurally with the Aurivillius Bi_2WO_6 phase, whereas the other polymorph crystallized isostructurally with Yb_2WO_6 in the monoclinic system. The SEM studies revealed both phases had a strong tendency to form agglomerates averaging nanometers in size. The photoluminescence emission spectra confirmed all of the samples were efficiently excited by near UV light and were dominated by the electric dipole transition $^5D_0 \rightarrow {}^7F_2$. The orthorhombic $Y_{2-x}Eu_xWO_6$ excitation spectrum possessed a broad band across the entire UV region (220–400 nm); therefore, $Y_{1.86}Eu_{0.14}WO_6$ could be considered an efficient spectral converter material for use in dye-sensitized solar cells.

1. Introduction

The chemistry of rare-earth elements plays an important role for both developing new solid-state lighting devices (SSLDs) and improving solar cells. The main rare-earth compound applications in these areas have focused on the development of luminescent materials or energy converters, also known as inorganic phosphors [1–4].

An inorganic phosphor typically consists of an inert host material, normally an oxide, nitride, fluoride, sulfide, or oxysulfide, doped with a small concentration of an activator ion, usually a rare-earth (*4f*) cation. Although the choice of activator ions and host matrix depends on the specific phosphor application, the crystal chemistry of the matrix restricts the choices available. In this sense, the ionic radius of the activator ion must be similar to that of the host cation for an appropriate substitution upon doping [5–7]. Activator ions may be classified into two broad categories. For the first, the energy levels of the dopant ions involved during emission interact weakly with the host lattice. Ln^{3+} ions are typical examples of this class of activator, and the optical transitions only involve the *4f* orbitals. For the second type of activator, *s* (Pb^{2+} or Sb^{3+}) or *d* (Mn^{2+} or Eu^{2+}) electrons are involved in the transition [8,9]. According to Jüstel et al., the strong electronic state coupling in the later yield lattice vibrations that lead to broad bands in the spectrum [1].

The host matrix is also important. The best host materials are divided into two types, optically inert and optically active; for optically inert hosts (oxides, silicates, phosphates, and fluorides), only the activator is involved during luminescence. Optically active anionic networks (tungstate and vanadate) are also involved in the luminescent process [10–12]. Therefore, rare-earth tungstates have attracted significant interest; alkali-metal rare-earth double tungstates, $ARE(WO_4)_2$ (A = Li^+, Na^+, K^+, RE = Gd^{3+}, La^{3+}, and Y^{3+}), in particular have been widely investigated due to their optical properties and excellent thermal and chemical stabilities [13–16]. Tungstates with different stoichiometries, such as Ln_2WO_6, have been studied less probably due to the difficulty with obtaining pure phases [17]. Yttrium tungstate with a formula of Y_2WO_6 is known to exhibit different crystallographic forms, monoclinic, tetragonal, etc., via the solid-state reaction at high temperature [18–21].

This paper is part of our continuing study on the synthesis, characterization, and luminescent properties of inorganic phosphors containing rare-earth cations [22–26]. In this report, we focused on the synthesis, characterization, and optical properties

* Corresponding author. Tel.: +56 55 2 355624.
E-mail address: jllanos@ucn.cl (J. Llanos).

http://dx.doi.org/10.1016/j.jallcom.2014.12.161
0925-8388/

of two different phases for the inorganic phosphor Y_2WO_6 doped with Eu^{3+}. The monoclinic form was prepared via a typical solid-state reaction, whereas the LT-phase was prepared via a low-temperature combustion synthesis [27,28]. The LT-phase exhibited broad absorption bands in the region from 250 to 390 nm, and emitted intense red visible light. These traits led us to propose LT-Y_2WO_6:Eu^{3+} as a potential spectral converter for dye-sensitized solar cells (DSSCs). The dopant ion concentration was also optimized.

2. Experimental

2.1. Synthesis

The monoclinic phase of Y_2WO_6:Eu^{3+} was prepared via a solid-state reaction at high temperature [27]. All phosphors were synthesized from a thoroughly ground mixture of the corresponding oxides, Y_2O_3, Eu_2O_3, and WO_3, in stoichiometric proportions. The mixtures were placed in an alumina boat and heated to 973 K for 10 h before cooling to below 400 K. The sample was removed from the crucible, ground into a powder, and reheated for 10 h at 1273 K. The procedure was repeated, and the sample was finally heated to 1373 K for another 10 h. All of these synthetic processes were performed under an air atmosphere.

Powder X-ray diffraction (PXD) data were collected using a Bruker D8 Advance diffractometer fitted with a graphite monochromator with Cu Kα radiation (λ = 1.54057 Å) across the range from $10 \leqslant 2\theta \leqslant 60$ to determine the phase purity. The experimental powder pattern for the doped and un-doped samples were almost in perfect agreement with those reported in the ICDS database and by Qin et al. and corresponded to the monoclinic phase of Y_2WO_6 [28,29].

In contrast, the orthorhombic LT-phase for Y_2WO_6:Eu^{3+} was prepared via a facile low-temperature combustion synthesis. Based on the stoichiometric formula, Y_2O_3 and Eu_2O_3, were dissolved in 10 ml of HNO_3 (2 mol dm^{-3}) under vigorous agitation at 353 K. The solution pH was adjusted to between 1 and 2. When the oxides dissolved completely, the solution pH was adjusted to pH ≅ 7. Meanwhile, 2.19 mmol of WO_3 (Aldrich 99.995% pure) was dissolved in 7 ml of NaOH (5 mol d m^{-3}) in another beaker with vigorous stirring at 353 K. The resultant $NaWO_4$ was dissolved in 5 ml of deionized water and mixed with 5 mmol of glycine. Both solutions were mixed to obtain a precursor suspension, which was concentrated in a beaker on a hot plate at 473 K with stirring. Reaching the critical temperature generated a small explosion accompanied by a large production of gases, which yielded a black product. Finally, the hot plate was turned off, and the sample was allowed to cool to room temperature. The product was ground in an agate mortar and annealed for 3 h at 673 K in a furnace. An optical inspection indicated the product was a homogeneous white powder. The experimental powder patterns agreed well with those reported in the literature [29].

2.2. Characterization

The phase purities were determined via an X-ray powder diffraction analysis (vide supra). The nanocrystalline $Y_{2-x}Eu_xWO_6$ phosphor surface morphologies were determined via scanning electron microscopy (SEM, Jeol, JSM-6360LV). The thermal stability of the samples (10.468 mg) was analyzed using a Netzsch STA 449 F3 Jupiter apparatus with a heating rate of 10 K/min. The photoluminescence (PL) spectra (emission and excitation) were measured using a JASCO FP-6500 spectrofluorometer. All of the spectra were collected at room temperature. The sample quantities were identical across all experiments so the photoluminescence intensities could be compared.

3. Results and discussion

The monoclinic phase: 10 compositions were synthesized for the $Y_{2-x}Eu_xWO_6$ system (x = 0.00; 0.02, 0.04, 0.06, 0.08, 0.10, 0.12, 0.14, 0.16, 0.18, and 0.20). The powder X-ray diffraction patterns for these compounds indicate all of the samples crystallized isostructurally with a monoclinic Y_2WO_6 structure with a P2/c space group (No. 13). The powder diffraction patterns for the monoclinic $Y_{2-x}Eu_xWO_6$ samples are shown in Fig. 1.

The Scherrer equation allows the crystallite size to be estimated. The Scherrer equation, $D = 0.90\lambda/\beta\cos\theta$, predicts the crystallite thickness for crystals smaller than 1000 Å because small angular differences are associated with large spatial distances (inverse space), so the diffraction peak broadening is expected to reflect the crystal size. In this equation, D is the average grain size, λ is the radiation wavelength used for the diffraction experiments,

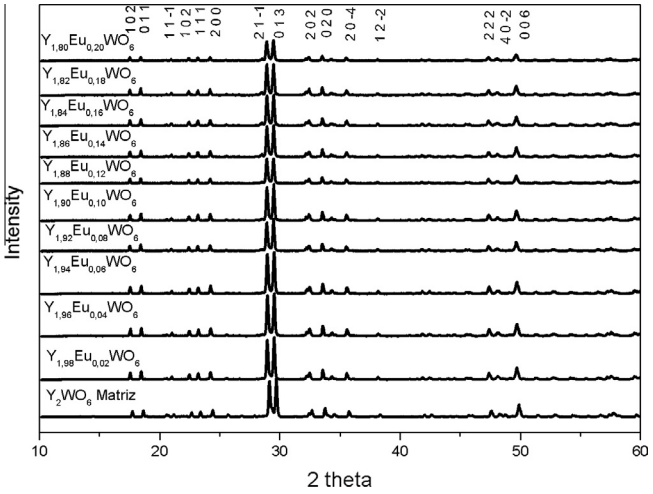

Fig. 1. XRD patterns of the monoclinic Y_2WO_6 doped with different concentration of Eu^{3+}.

θ is the diffraction angle, and β is the full-width at half maximum (FWHM) for the observed peaks [30,31]. The strongest diffraction peak (0 1 3) was used to calculate the sample grain size. Our results indicate the crystallite sizes for monoclinic $Y_{2-x}Eu_xWO_6$ ranged from 60 to 85 nm.

The crystallite morphology for monoclinic $Y_{2-x}Eu_xWO_6$ was inspected via scanning electron microscopy (SEM). This study revealed the samples were spherical with a strong tendency to form aggregates as shown in Fig. 2.

The excitation spectrum for monoclinic $Y_{2-x}Eu_xWO_6$ (shown in Fig. 3) exhibited a broad C–T band centered at 300 nm along with sharp $^7F_0 \rightarrow {}^5L_6$ (395 nm) and $^7F_0 \rightarrow {}^5D_2$ (465 nm) transitions. The C–T band intensity is much larger than the $f \rightarrow f$ transitions. The broad, intense band consisted of overlaying O^{2-}–Eu^{3+} and O^{2-}–W^{6+} charge transfer bands.

The emission spectra for the monoclinic samples were dominated by the red peak due to the electric dipole transition in $Y_{2-x}Eu_xWO_6$ at a wavelength of 300 nm, and an intense peak occurred at 611 nm. All of the spectra exhibited similar features, and the characteristic emission originated from the transition between the $^5D_0$ excited state to the ^7F_j ground state (j = 0, 1, 2, 3 and 4) for the $4f^6$ configuration of Eu^{3+}. The optimal Eu^{3+} doping concentration in the host was x = 0.14 as shown in Fig. 4. The PL

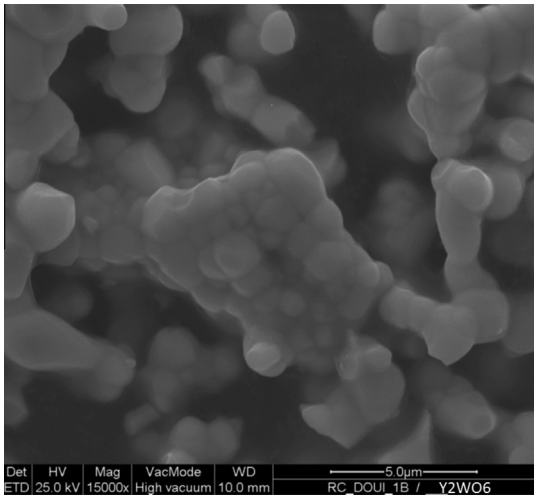

Fig. 2. SEM micrography of $Y_{1.86}Eu_{0.14}WO_6$ prepared by solid-state reaction.

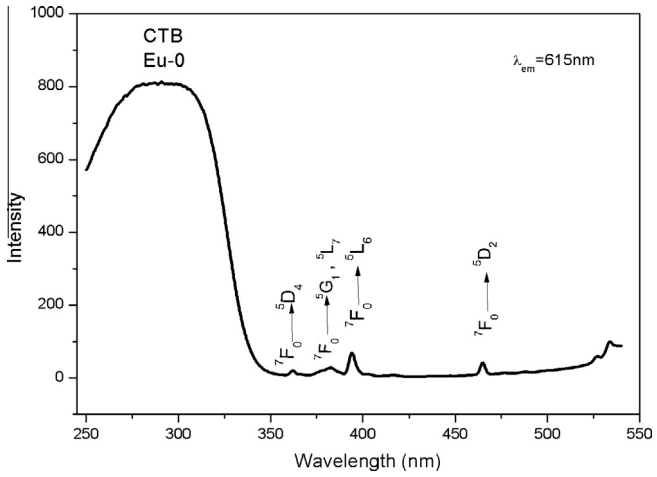

Fig. 3. Excitation spectrum of the phosphor $Y_{1.86}Eu_{0.14}WO_6$ (monoclinic phase) at room temperature (λ_{em} = 615 nm).

intensity decreased when x exceeded 0.14 due to concentration quenching, which is related to an energy transfer between activator centers. Therefore, determining the critical R_c distance, that is, the critical distance between the donor (activator) and acceptor (quenching site), is necessary. The critical distance can be estimated from the equation proposed by Blasse et al. [32]:

$$R_c \approx 2\left(\frac{3V}{4\pi x_c N}\right)^{\frac{1}{3}}$$

where R_c = the critical distance, V = the unit cell volume, x_c = the critical concentration, N = the *number* of formula units in the unit cell. Because V = 523.6 Å^3, x_c = 7%, and N = 4, the critical distance R_c = 11.3 Å. This result indicates the Eu^{3+} ions are localized randomly in the host crystal structure and rules out the possibility of clusters.

For the orthorhombic LT-phase for Y_2WO_6:Eu^{3+}, the X-ray powder diffraction patterns for LT-$Y_{2-x}Eu_xWO_6$, (x = 0.02, 0.06, 0.10, 0.14, and 0.18) indicated all of the phosphors crystallized isostructurally with the Aurivillius phase, Bi_2WO_6, which crystallizes with the orthorhombic space group $P2_1ab$. This structure is layered with perovskite-like WO_6 slabs [33–35]. The effect of the Y^{3+} substitution on the Bi_2WO_6 was exemplified by the clear shifting in PXRD reflections. The shift towards bigger 2θ value was closely related to the ionic radii for Y^{3+} and Bi^{3+}. According to Shannon the ionic radii are 1.03 Å for Bi^{3+} and 0.9 Å for Y^{3+}, which are both hexa-coordinates [36]. In contrast, replacing Y^{3+} with Eu^{3+} in the structure produces slightly smaller 2θ values. The ionic radius hexa-coordinate for Eu^{3+} is 0.94 Å. The powder diffraction patterns for LT-$Y_{2-x}Eu_xWO_6$ and Bi_2WO_6 are shown in Fig. 5. The strongest diffraction peak (1 1 3) was used to calculate the grain size for all of the samples using the Scherrer equation [30,31]. In this case, the crystallite sizes in the compounds ranged from 18 to 30 nm ($D_{Y1.98Eu0.02WO6}$ = 29 nm; $D_{Y1.90Eu0.10WO6}$ = 27 nm; $D_{Y1.94Eu0.06WO6}$ = 22 nm; $D_{Y1.86Eu0.14WO6}$ = 19 nm; $D_{Y1.82Eu0.18WO6}$ = 19 nm).

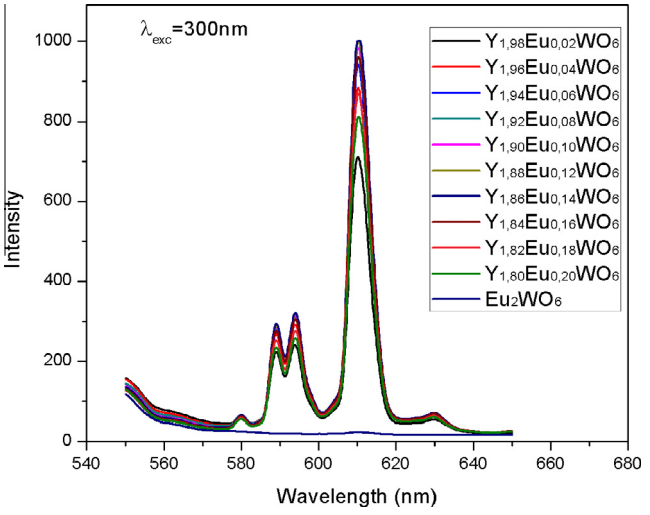

Fig. 4. Emission spectra of the monoclinic phase $Y_{2-x}Eu_xWO_6$ (x = 0.00; 0.02; 0.04; 0.06; 0.08; 0.10; 0.12; 0.14; 0.16; 0.18; 0.20) prepared by solid-state reaction (λ_{exc} = 270 nm).

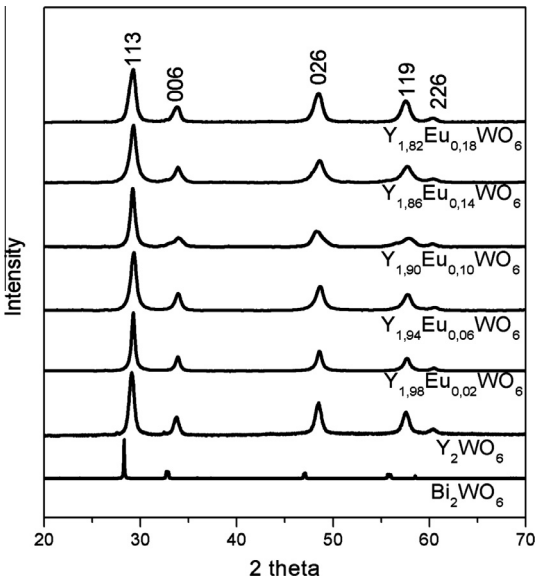

Fig. 5. XRD patterns of the Aurivillius phases $Y_{2-x}Eu_xWO_6$ and Bi_2WO_6.

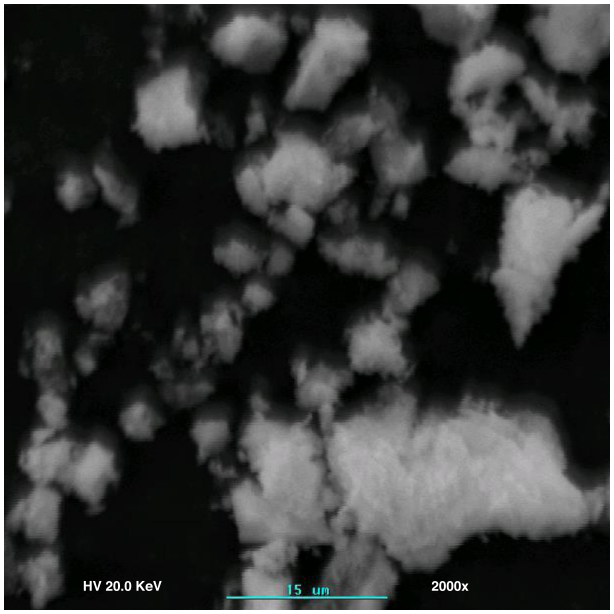

Fig. 6. SEM micrography of the $Y_{1.86}Eu_{0.14}WO_6$ (Aurivillius phase) prepared by low-temperature method.

The crystallite morphology for these phosphors were determined via scanning electron microscopy (SEM). The SEM studies

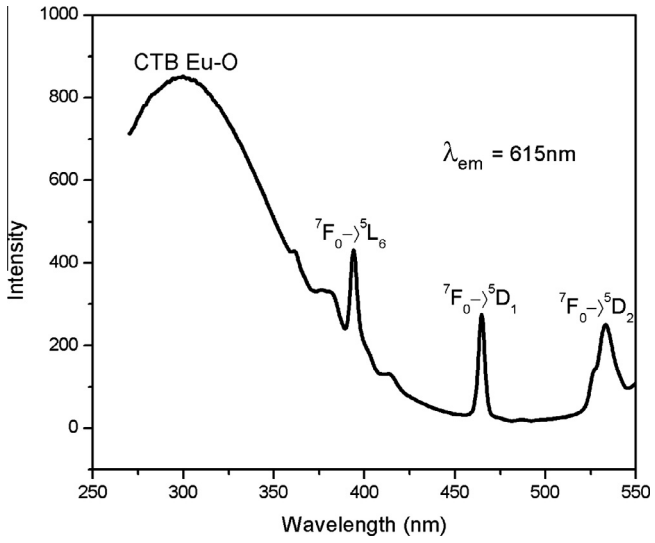

Fig. 7. Excitation spectrum of the orthorhombic phosphor $Y_{1.86}Eu_{0.14}WO_6$ (λ_{em} = 614 nm).

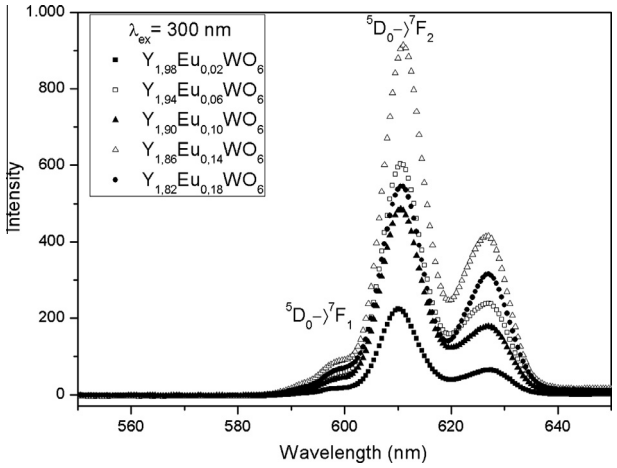

Fig. 8. Emission spectra of the Aurivillius phases $Y_{2-x}Eu_xWO_6$ (x = 0.02; 0.04; 0.06; 0.08) (λ_{exc} = 300 nm).

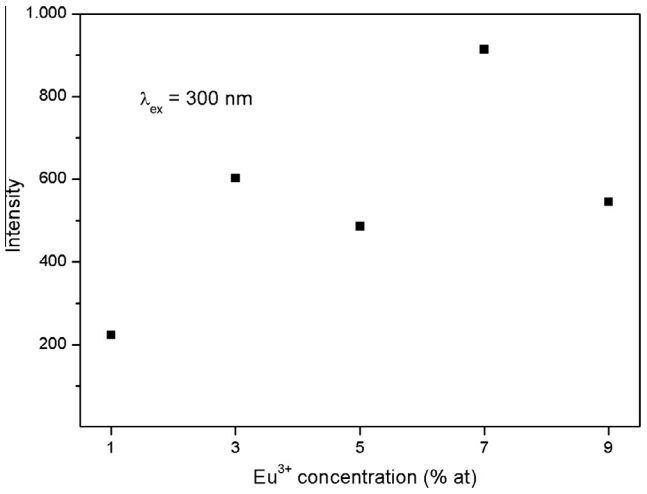

Fig. 9. The dependence of the emission intensity against the Eu^{3+}concentration in the Aurivillius phosphor phase.

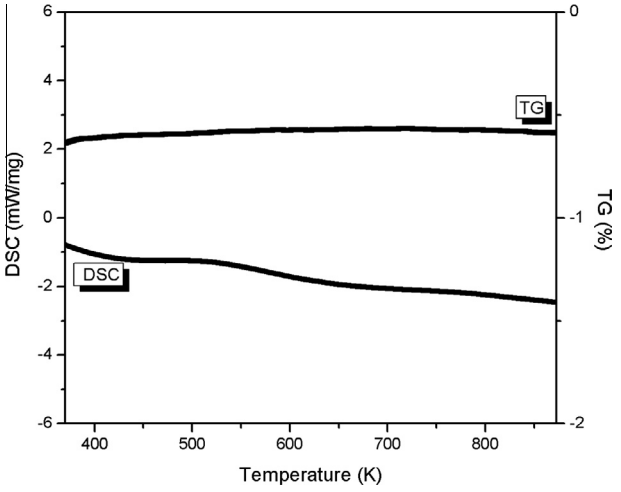

Fig. 10. DSC curve of the orthorhombic $Y_{1.86}Eu_{0.14}WO_6$ phosphor.

indicated the samples strongly tended to form agglomerates with a spongy appearance as shown in Fig. 6.

The excitation spectrum for LT-$Y_{2-x}Eu_xWO_6$ is shown in Fig. 7. This spectrum was obtained by monitoring the red emission at 614 nm from Eu^{3+}. As shown in Fig. 7, the excitation spectrum contained a broad CT band centered at approximately 300 nm and included sharp $^7F_0 \rightarrow {}^5L_6$ (395 nm), $^7F_0 \rightarrow {}^5D_1$ and $^7F_0 \rightarrow {}^5D_2$ transitions. The intensity for the charge transfer band (Eu-O) was greater than for the *f–f* transitions. An interesting feature of the CTB is its extended tail into the near UV range, which is similar to the observed excitation spectrum for some vanadates [16].

As Fig. 8 illustrates, the emission spectra for all of the samples were dominated by the red peak due to the electric dipole transition $^5D_0 \rightarrow {}^5F_2$ at 614 nm, which indicates the Eu^{3+} ions randomly occupy the two crystallographic positions characterized by the lack of inversion point [11]. The strong $^5D_0 \rightarrow {}^5F_2$ emission line intensity increased with increasing Eu^{3+} concentration up to 7%. The concentration dependence for the Eu^{3+} emission intensity is shown in Fig. 9. Concentration quenching was observed once the rare-earth concentration increased above 7%. At this point, the distance between the emitter centers decreased, and forming Eu^{3+} clusters or pairs becomes possible. The critical distance calculated from the Blasse equation was 9.18 Å [32].

The simultaneous thermal analyses (TG/DSC) co the most efficient phosphor, $Y_{1.86}Eu_{0.14}WO_6$, was performed up to 873 K. Fig. 10 shows that during the process the mass only changed 5 μg, which demonstrates an excellent long-term stability for the as-prepared orthorhombic phosphor.

The as-prepared phosphors can be used as ultraviolet–absorbing luminescent converters to improve the light-harvesting process in dye-sensitized solar cells (DSSCs) and increase the photocurrent. This type of phosphor could be promising because of its broad band from 250 to 380 nm. UV irradiation is known to be harmful to DSSC because the dye rapidly oxidizes, and the electrolyte is irreversibly degrades [14,37]. Further work is in progress to incorporate these phosphors into DSSC and measure the photovoltaic parameters.

4. Conclusions

Two different $Y_{2-x}Eu_xWO_6$ phases were successful synthesized, the monoclinic phase via a classic solid-state reaction at high temperature and the orthorhombic phase via a facile low-temperature combustion reaction, and their luminescent properties were

investigated. A red peak due to an electric dipole transition dominates the emission spectra for both phases. The excitation spectra were dominated by the Eu–O CTB; however, the excitation band for the orthorhombic phase broadened to a longer wavelength. Both red phosphors can be used as either energy converters in SSLDs with InGaN-based LED as the excitation source or as ultraviolet–absorbing luminescent converters to improve the light harvesting process for dye-sensitized solar cells (DSSCs).

Acknowledgments

This work was financially supported by a Grant from FONDECYT (Chile), No. 1130248; D.E. acknowledges CONICYT for providing a doctoral fellowship.

References

[1] T. Jüstel, H. Nikols, C. Ronda, Angew. Chem. Int. Ed. 37 (1998) 3084.
[2] J.T. Ingle, R.P. Sonekar, S.K. Omanwar, Y. Wang, L. Zhao, J. Alloys Comp. 608 (2014) 235.
[3] H. Höppe, Angew. Chem. Int. Ed. 48 (2009) 3572.
[4] J. Llanos, R. Castillo, D. Espinoza, R. Olivares, I. Brito, J. Alloys Comp. 509 (2011) 5295.
[5] G. Blasse, B.C. Grabmaier, Photoluminescent Materials, Springer Verlag, Berlin, 1984.
[6] J. Silver, R. Withnall, Chem. Rev. 106 (2004) 2833.
[7] C.L. Lo, J.-G. Duh, B.S. Chiou, C.-C. Peng, L. Ozawa, Mater. Chem. Phys. 71 (2001) 179.
[8] P. Alemany, I.de P.R. Moreira, R. Castillo, J. Llanos, J. Alloys Comp. 513 (2012) 630.
[9] C. Song, B. Chen, Y. Chen, Y. Wu, Z. Zhuang, X. Lu, X. Qiao, X. Fan, J. Alloys Comp. 590 (2014) 546.
[10] G. Seeta Rama Raju, S. Buddhudu, Mater. Lett. 62 (2008) 1259.
[11] G. Gundiah, Y. Shimomura, N. Kijima, A.K. Cheetham, Chem. Phys. Lett. 445 (2008) 1259.
[12] H. Wang, W. Lu, Z. Yi, L. Rao, S. Zeng, Z. Li, J. Alloys Comp. 618 (2015) 776.
[13] Y. Huang, Y. Fenh, W. Zhu, Appl. Phys. A80 (2005) 409.
[14] J. Liu, Q. Yao, Y. Li, Appl. Phys. Lett. 88 (2006) 173119.
[15] X. Yu, Y. Qin, M. Gao, L. Duan, Z. Jiang, L. Gou, P. Zhao, Z. Li, J. Lumin. 153 (2014) 1.
[16] L. Zhou, J. Huang, F. Gong, Y. Lan, Z. Tong, J. Sun, J. Alloys Comp. 495 (2010) 268.
[17] J. Huang, J. Xu, H. Li, H. Luo, X. Yu, X. Li, J. Solid State Chem. 184 (2011) 843.
[18] H.J. Borchardt, Inorg. Chem. 2 (1963) 170.
[19] H. Ruonan, M. Qingyu, L. Wei, L. Hongling, J. Rare Earth 31 (2013) 864.
[20] J. Huang, J. Xu, H. Li, H. Luo, X. Yu, Y. Li, J. Solid State Chem. 184 (2011) 843.
[21] J. Wang, Z. Zhang, J. Zhao, H. Chen, X. Yang, Y. Tao, Y. Huang, J. Mater. Chem. 20 (2010) 10894.
[22] S. Fuentes, N. Barraza, E. Veloso, R. Villarroel, J. Llanos, J. Alloys Comp. 569 (2013) 52.
[23] J. Llanos, R. Castillo, J. Lumin. 129 (2009) 465.
[24] J. Llanos, R. Cortes, Mater. Res. Bull. 43 (2008) 2763.
[25] J. Llanos, R. Castillo, J. Lumin. 1309 (2010) 465.
[26] J. Llanos, R. Castillo, I.R. Martin, L.L. Martin, P. Haro-Gonzalez, J. Gonzalez-Platas, J. Lumin. 145 (2014) 553.
[27] Z. Zhang, W. Wang, M. Shang, W. Yin, J. Hazard. Mater. 177 (2010) 1013.
[28] C. Qin, Y. Huang, G. Chen, L. Shi, X. Qiao, J. Gan, H.J. Seo, Mater. Lett. 63 (2008) 1162.
[29] N.A. McDowell, K.S. Knight, P. Lightfood, Chem. Eur. J. 12 (2006) 1493.
[30] A.L. Patterson, Phys. Rev. 56 (1939) 978.
[31] Y.W. Zhang, Y. Yang, S. Jin, S.J. Tian, G.B. Li, J.T. Jia, C.S. Liao, C.H. Yan, Chem. Mater. 13 (2001) 372.
[32] S.H.M. Poort, W.P. Blokpoel, G. Blasse, Chem. Mater. 7 (1995) 1547.
[33] B. Aurivillius, Ark. Kemmi 1 (1949) 463.
[34] H. Djani, P. Hermet, P. Ghosez, J. Phys. Chem. 118 (2014) 13514.
[35] V.I. Voronkova, E.P. Kharitonova, O.G. Rudnitskaya, J. Alloys Comp. 487 (2009) 274.
[36] R.D. Shannon, Acta Cryst. A32 (1976) 751.
[37] A. Kay, M. Graetzel, Chem. Mater. 14 (2002) 2930.